Sodium diffusion in ionic liquid-based electrolytes for Na-ion batteries: The effect of polarizable force fields

22 December 2025

Sodium diffusion in ionic liquid-based electrolytes for Na-ion batteries: the effect of polarizable force fields

Arianna Massaro,[1,2] Jocasta Avila,[2] Kateryna Goloviznina,[2] Ivan Rivalta,[2,3] Claudio Gerbaldi,[4] Michele Pavone,[1] Margarida F. Costa Gomes,[2] and Agilio A. H. Pádua[2, a)]

[1)] *Department of Chemical Sciences, Università di Napoli "Federico II", via Cintia 26, 80126 Naples, Italy*

[2)] *Univ Lyon, Ens de Lyon, CNRS UMR 5182, Université Claude Bernard Lyon 1, Laboratoire de Chimie, F69342, Lyon, France*

[3)] *Dipartimento di Chimica Industriale "Toso Montanari", Università degli Studi di Bologna, Viale del Risorgimento 4, I-40136 Bologna, Italy*

[4)] *GAME Lab, Department of Applied Science and Technology (DISAT), Politecnico di Torino, 10129 Torino, Italy*

Understanding the transport of sodium ion in ionic liquids is key to design novel electrolyte materials for sodium-ion batteries. In this work, we combine molecular dynamics simulation and experiments to study how molecular interactions and local ordering affect relevant physico-chemical properties. Ionic transport and local solvation environments are investigated in electrolytes composed of sodium bis(fluorosulfonyl)imide, (Na[FSI], in N,N-methylpropylpyrrolidinium bis(fluorosulfonyl)imide, [C$_3$C$_1$pyr][FSI], at different salt concentrations. The electrolyte systems are modelled by means of molecular dynamic simulations using a polarizable force field. We show that including polarization effects explicitly in the molecular simulations is required in order to attain a reliable description of the transport properties of sodium in the [C$_3$C$_1$pyr][FSI] electrolyte. Validation of the computational results by comparison to experimental data allows to assess the suitability of polarizable force fields in describing and interpreting the structure and the dynamics of the sodium salt-ionic liquid system, which is essential to enable the application of IL-based electrolytes in novel energy-storage technologies.

Keywords: Na-ion batteries, ionic liquid electrolytes, molecular dynamics simulations, polarizable force field.

---

[a] Electronic mail: agilio.padua@ens-lyon.fr

I. INTRODUCTION

Energy-storage systems are essential for the transition toward a sustainable society.[1] In this context, electrochemical devices, such as rechargeable batteries, represent a major storage technology since they can efficiently store and deliver energy on demand in combination with renewable sources. Lithium-ion batteries (LIBs) have had tremendous technological and social impact, recognized by the 2019 Nobel Prize in Chemistry.[2,3] More recently, Na-ion batteries (NIBs) have been considered as promising alternatives to LIBs for smart-grid applications.[4,5] In fact, the natural abundance of sodium should ensure a remarkable price drop, which would favor their rapid intrusion in the market of large-scale energy storage from renewables. The similar operating principles with LIBs has enabled remarkably quick advances in the development of NIBs, although significant improvements in both electrode and electrolyte materials are still needed.[6,7] Concerning electrolytes, current challenges are related to safety and recycling issues. New classes of electrolytes, such as solid polymer matrices[8] and room-temperature ionic liquids (RTILs),[9] can replace the currently-used liquid electrolytes in several formulations.[10,11] RTILs emerged as valid alternatives to common organic solvents because of their unique properties, including virtually no volatility, non-flammability, high thermal and electrochemical stability, that would enhance the sustainability of manufacture processes, the device operation and cycle life. Since the discovery of the first ionic liquid,[12] the interest for this family of materials increased strongly in both academia and industry,[13] covering a wide range of applications, from solvents for reactions, separations and materials processing,[14,15] to electrolytes for energy-storage devices,[16] but also lubricants[17] or plasticisers.[18] RTILs are low-melting organic salts and highly structured fluids with complex interactions arising from the variety of chemical groups composing the ions. Modelling these complex interactions and understanding how molecular structure determines the properties of these materials are key to a rational design of new materials for energy-storage devices.

Significant efforts have been carried out to investigate physical and chemical properties, such as viscosity and ionic conductivity, that are directly related to ion transport and, thus, to electrochemical performance.[19–29] Atomistic molecular dynamics (MD) appears as a highly suitable methodology to establish structure-property relations for IL-based electrolytes from a molecular-scale view. MD is based on a detailed description of the molecular structures

and interactions (the atomistic force field) and covers ranges of time (10 to 100 ns) and length (10 to 100 nm) scales that are suited to the study of microscopic ordering, dynamics and energetics of condensed phases,[19,20] treated as extended systems with periodic boundary conditions. At the present state-of-the art in theoretical methods and computational power, quantum mechanical calculations with the required accuracy would be limited and not affordable in computational cost for the aforementioned time and length scales that typically characterize the ordering and dynamics of ionic liquids. MD simulations of RTILs have led to the awareness that both structure and dynamics are very sensitive to the representation of electrostatic interactions. Both equilibrium and transport properties in these systems strongly depend on details of non-covalent interactions, namely the balance between Coulomb and van der Waals forces.[21–23]

Describing Coulomb interactions by means of fixed partial charges on the atomic sites (with integer ionic charges) is common practice in atomistic force fields and has been successful in predicting thermodynamic properties. However, the dynamics turns out to be too slow (viscosity too high) when compared to experiments.[24] One possible workaround has been to scale ionic charges (and thus each atomic partial charge) by a factor of about 0.8.[25–27] Such a scheme allows faster dynamics due to the diminished Coulomb interactions, but the reduction in cohesive energy leads to issues with structural and volumetric properties, namely the density will become too low and features of near-neighbour structure will become attenuated.[29]

The possibility of including explicit polarization in classical atomistic force fields for ionic liquids has changed this scenario recently, bringing significant improvements in the predictive power of MD simulations.[28] This approach is at the boundary between quantum (electronic structure) and classical levels, since it represents the response of electron clouds (via charge distributions) to their electrostatic environment. In ionic liquids, composed of large molecular ions, polarizability is expected to play an important role in adjusting the electron density and thus an explicit treatment of induction should greatly improve models.[29]

Herein, we present an application of a polarizable model for a mixed salt-RTIL system (Na[FSI] + [C_3C_1pyr][FSI]) which is of particular interest for Na-ion battery applications. We investigate physico-chemical properties that can be relevant to assess its suitability as an electrolyte for NIBs, and we specifically add explicit polarization to attain a reliable description of sodium transport properties in the ionic liquid. We provide insights from MD

4

simulations together with original experimental results that are used to validate the theoretical predictions. Despite its lower thermal and electrochemical stability when compared to its [TFSI] counterpart, the [C$_3$C$_1$pyr][FSI] ionic liquid has been widely used in batteries, mainly LIBs, due to its remarkable SEI-forming ability and lower viscosity accounting for enhanced ionic conductivity;[30–32] still, ongoing efforts are focused on the understanding of ion transport characteristics. Actually, gaining a proper understanding of the fundamental chemistry that occurs upon addition of the sodium salt to the ionic liquid to predict its speciation and interactions with the bulk solvent is fundamental to develop advanced, high-performing NIB systems employing IL-based electrolytes. In this respect, Chen *et al.*[33] recently reported an extensive study on the same salt-IL system at different salt concentrations and showed an unexpected behaviour of Na$^+$ diffusion as a function of concentration. According to the Walden rule (eq. 1), ionic conductivity, Λ, (which accounts for ion mobility) should be roughly inversely proportional to viscosity, η, for the same ions in different solvents.

$$\Lambda\eta = \text{const.} \tag{1}$$

The study of Chen *et al.*[33] reported non-monotonous diffusion coefficients of Na$^+$ as a function of concentration in [C$_3$C$_1$pyr][FSI], despite one would expect that with increasing Na salt concentration the viscosity increases and consequently ion diffusion slows down monotonously. Thus, only some marked association or solvation interactions imparting a strong deviation onto the dynamics of sodium could justify such behaviour. Since the work of Chen *et al.*[33] was performed using fixed, scaled-charge force fields, this motivated us in the present work to inquire if similar results on the same [FSI]-based salt-RTIL system could be also observed using a polarizable force field.

Hence, we report results and interpretation of sodium diffusion in [C$_3$C$_1$pyr][FSI] by comparing theoretical results obtained from fixed scaled-charges and by polarizable force fields, in order to evaluate the effect of polarization. We also provide a direct comparison of the computed physico-chemical properties with experimental data, including density, viscosity and diffusion coefficients measured by DOSY-NMR technique.

5

II. MATERIALS AND METHODS

Materials. The ionic liquid N-propyl-N-methyl pyrrolidinium bis(fluorosulfonyl)imide ($[C_3C_1pyr][FSI]$) was purchased from Solvionic 99.5 % pure. The ionic liquid was degassed under primary vacuum for 48 h and was kept dried and degassed inside a glove box (Jacomex GP Campus) before sample preparation. Sodium bis(fluorosulfonyl)imide (Na[FSI]) was purchased from Solvionic 99.7 % pure. Before utilization, the salt was kept inside the glove box and used without further treatment. Deuterated chloroform ($CDCl_3$) 99.80 % for NMR, was purchased from Eurisotop with a water content below 0.01 %.

Sample preparation. $Na[FSI]+[C_3C_1pyr][FSI]$ solutions were prepared inside the glove box at room temperature by weighing the components using a New Classic MS Mettler Toledo balance with an accuracy of ±0.01 mg and shaking by hand the flask for 5 to 10 min.

To record the NMR spectra, the samples were placed in NMR tubes and degassed under primary vacuum for over 1 h before each measurement. The NMR spectra of the pure ionic liquid and of $Na[FSI]+[C_3C_1pyr][FSI]$ solutions were carried out using $CDCl_3$. To avoid changes in composition, an inner coaxial tube (5 mm diameter) containing the deuterated solvent was used. The same inner tube was used with all the samples in order to avoid spectral differences due to the magnetic susceptibility of the material.

Force field. We used the CL&Pol force field for ionic liquids,[24,29] which is a polarizable version of the widely adopted CL&P fixed-charges model.[22,23] The CL&Pol force field uses Drude induced dipoles[34] which, placed on each atomic site, represent the induction effects. The induced dipoles are formed by an additional point charge, the Drude particle (DP), and its opposite charge, the Drude core (DC), placed on the atom. The DP and DC are linked by a harmonic bond of equilibrium length 0 and the Coulomb interactions between each DC and its DP are excluded from computation of energies and forces. The DP carries a charge q_D and the DC a charge $q - q_D$, where q is the total charge of the atom. The extension of the harmonic springs allows the Drude dipoles to respond to the local electric field. We followed the approach of Lamoureux and Roux[35] in assuming a global force constant of $k_D = 4184$ kJ mol^{-1} Å^{-2} for the DC–DP bonds and determining q_D values from the atomic polarizabilities, $\alpha = q_D^2/k_D$. We adopted induced dipoles with a positive charge q_D on the DP, which enables more robust trajectories in the presence of the high positive charge density on the Na ion. In our systems, negative Drude particles would create more risks of

a polarization catastrophe, with Drude particles being pulled too far away from their cores. We did not apply any additional constraints[36] or damping functions to limit the motion of the DP.

The force field parameters necessary to take into account polarization effects were obtained from ab initio calculations of induction (polarization) and dispersion energies, using symmetry-adapted perturbation theory (SAPT).[29] These detailed calculations were performed for a set of molecular fragments including common cation and anion head-groups, side chains and molecular solvents. The systems considered here were built from those fragments, namely $C_3C_1pyr^+$ was represented by the cation head group, $C_1C_1pyr^+$, with sites in the alkyl chain derived from the C_4H_{10} fragment. With polarization being taken into account explicitly by the Drude induced dipoles, the CL&Pol model uses van der Waals (or Lennard-Jones) parameters from original (non-polarizable) CL&P model, rescaled on the basis of the relative contributions of dispersion and induction energies obtained from SAPT. In this manner, in the polarizable force field the Lennard-Jones potential terms account only for repulsive and dispersive interactions, and not for induction implicitly. The k-factors[29] used here to obtain the Lennard-Jones terms in the polarizable force field are fragment-based and have the following values: k(pyr-FSI) = 0.54, k(pyr-CC) = 0.67, k(FSI-CC) = 0.77, where CC stands for the Cβ and Cγ atoms (and respective H atoms) in the alkyl side chain of the pyrrolidinium cation.

In all, the additional information at the molecular level required to parameterize a polarizable force field (from a fixed-charge one) are the relative weight of induction versus dispersion terms, obtained from SAPT calculations, and atomic polarizabilities, which we took from the recent literature.[37]

In order to set up non-polarizable simulations for comparison, we modified the electrostatic contribution in the CL&P force field by scaling down the atomic charges by a factor of 0.8,[25] which is a simple fix that improves calculation of transport properties (at the cost of worsening the density values and structural quantities).

Molecular dynamics simulations. Drude induced dipoles have been implemented in major molecular dynamics codes, including the LAMMPS code,[38,39] which we used for the present simulations. The additional degrees of freedom corresponding to the relative motion of the DP with respect to their cores are handled by a separate thermostat in order to keep these modes at very low temperature,[35,39] thus closely matching the trajectories

of relaxed induced dipoles. We built 5 simulation boxes containing 216 ion pairs for the mixed Na[FSI]+[C$_3$C$_1$pyr][FSI] system, with a series of salt concentrations ($x_{\text{Na[FSI]}}$ of 0.0, 0.1, 0.3, 0.5 and 0.9, with x denoting mole fraction). Initial configurations were generated using the fftool[40] and packmol[41] utilities. A cutoff distance of 12 Å was considered for the Lennard-Jones potential and for the real-space part of electrostatics. The particle-particle particle-mesh method was used to evaluate electrostatic energies with an accuracy of 1×10^{-4}. Hydrogen-terminating bonds were constrained using the SHAKE algorithm. The time step was set to 1 fs. After initial 0.5 ns equilibration runs, we collected 8 ns NpT trajectories, regulated by Nosé-Hoover thermostat and barostat, with temperature being set at 353 K and pressure at 1 bar, for comparison with experimental data from the literature.[30]

Density and viscosity measurements. Density and viscosity were measured in a coupled Anton Paar densimeter (DMA 5000 M) and viscometer (LOVIS 2000 ME). In the densimeter, a U-shaped vibrating-tube is electronically excited at its characteristic frequency, which depends on the density of the sample inside. Calibration of the instrument was performed using two substances of precisely known densities: air and ultra-pure water (density standard provided by Anton Paar). The precision and accuracy of the measurements are 5×10^{-6} g cm^{-3} and 7×10^{-6} g cm^{-3}, respectively, in density and 0.01 °C in temperature. The viscometer is based on the Hoeppler falling ball principle, according to which the rolling time of a ball through the liquid confined in a glass capillary is determined. In order to cover the viscosity range of our samples in the working temperature range, two capillaries with different diameters, 1.8 mm and 2.5 mm, and two balls of the same material, were calibrated with two different standard oils, APN26 and APN415, respectively. The precision and accuracy of the measurements are 0.05 and 0.5 %, respectively, in viscosity and 0.02 °C in temperature. Both the densimeter and viscometer cells were filled with *ca.* 1 mL of sample and the measurements carried out simultaneously, using the temperature-table scan mode at atmospheric pressure and in the temperature range 293.15 to 353.15 K.

NMR experiments. NMR experiments were carried out on a Bruker Avance 400 MHz spectrometer equipped with a diffusion probe BBdiff with Z gradients up to 2.8 T m^{-1} at 10 Å. The self-diffusion coefficients of the species in each sample were determined through ^{1}H and ^{19}F pulsed-field-gradient spin-echo NMR experiments (PFGSE), using a bipolar-pulse longitudinal eddy current delay (BBPLED) pulse sequence. The temperature was regulated at 298 K and a coaxial insert containing the deuterated solvent was used to lock and adjust

the chemical shift scale. For each PFGSE experiment, the pulse gradient and diffusion time were optimized in order to get a signal attenuation of about $95\,\%$. The relaxation delay was set to $1.5\,$s and 8 scans were acquired for each measurement. Rectangular pulse field gradients shaped with smoothed edges (SMSQ10.100) were used with a length δ going from 0.8 to $2.5\,$ms for ^{1}H experiments and from 1.5 to $2.5\,$ms for ^{19}F experiments. The intensity of the gradient was linearly incremented from 5.26 to $258.06\,$G cm^{-1} for ^{1}H-NMR experiments and from 3.72 to $182.50\,$G cm^{-1} for ^{19}F-NMR ones. Data were processed using the Topspin v3.6 software and diffusion curves were fitted using DynamicsCenter, implemented in Topspin.

III.   RESULTS AND DISCUSSION

A.   Dynamic properties

Self-diffusion coefficients were calculated from mean-squared displacements (MSD) using the Einstein relation:

$$D = \lim_{t \to \infty} \frac{1}{6} \frac{d}{dt} \langle (r(t) - r(0))^2 \rangle \tag{2}$$

We extracted the MSD of $C_3C_1pyr^+$ and FSI^- from the $8\,$ns-trajectory of the pure RTIL and linearly fitted the plot in its diffusive regime (from 2 to $8\,$ns, see Figure S1).[42] We then computed the self-diffusion coefficients according to Equation (2). The results obtained from both fixed scaled-charges and polarizable trajectories are reported in Table I.

Table I. Density, ρ, and self-diffusion coefficients, $D_{C_3C_1pyr^+}$ and D_{FSI^-}, calculated with both fixed scaled-charges (ScaleQ) and polarizable force fields (Drude). Experimental data from the literature are reported for comparison.

Method	ρ (g cm^{-3})	$D_{C_3C_1pyr^+}$ (m^2 s^{-1})	D_{FSI^-} (m^2 s^{-1})
exp[43]	1.295	14.0×10^{-11}	17.0×10^{-11}
ScaleQ	1.254	2.71×10^{-11}	3.20×10^{-11}
Drude	1.275	7.08×10^{-11}	7.84×10^{-11}

From the values listed in Table I we can confirm that the polarizable model gives more reliable predictions of both density and diffusion compared to the fixed scaled-charges one,

showing better agreement with experimental data reported in the literature:[43] the deviation from experimental density are $-1.5\,\%$ and $-3.2\,\%$ for Drude and ScaleQ models, respectively; self-diffusion coefficients are lower than the experimental ones by a factor of 2 in the case of Drude model, while even lower (by factor of 5 to 6) in the case of fixed scaled-charges force field.

We then moved to the binary salt-ionic liquid system and compute the self-diffusion coefficients of the ions that are present in the solutions. The results obtained with the polarizable model are shown in Figure 1 (see Table S1 for comparison with the ScaleQ results). For each ionic species, we observe a monotonous decrease of self-diffusion coefficients as a function of salt concentration, consistently with the Walden rule (Equation 1).
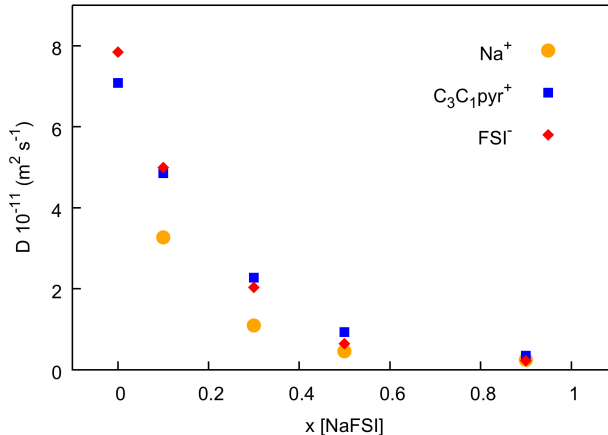

Figure 1. Plot of self-diffusion coefficients, D, as function of composition, x [NaFSI], computed for each ionic species from MD simulations using the polarizable force field.

In order to validate our theoretical results obtained from MD simulations using the polarizable force field, we provide here direct comparison to experimental results. Despite extensive characterization of these systems already exists and several experimental data have been previously reported in the literature,[43–45] we set up density, viscosity and diffusion coefficients experiments in order to have a more systematic and precise experimental reference for our theoretical outcomes. Self-diffusion coefficients of $C_3C_1pyr^+$ and FSI^- ions are obtained by DOSY-NMR technique at room temperature, while density and viscosity have been determined in a wide temperature range, so that in principle diffusion coefficients at any other temperature could be extrapolated for direct comparison to MD simulations. We will discuss this approach later in the text.

For the samples prepared as indicated in Table S2, we measured density and viscosity and report the results in Figure 2. Density data have been linearly fitted as a function of temperature, presenting an absolute average deviation from the fits lying between 0.007% and 0.01% (see Tables S3 and S5 for details). Viscosity data (reported in Figure 2(b) as the log of viscosity, where viscosity is given in mPa s) have been fitted using the Vogel-Fulcher-Tammann-Hesse (VFTH) equation,[46] with an absolute average deviation lying between 0.1% and 4%(see Tables S4 and S5 for details). Both density and viscosity naturally decrease with the temperature in each solution, while an increasing trend with the salt concentration is shown at all temperatures: higher values are observed going from the pure ionic liquid (black line) and the solution containing $x = 0.1$ Na salt (pink line), while a pronounced increase is detected from $x = 0.1$ to $x = 0.3$ (green line) and even more from $x = 0.3$ to $x = 0.5$ (blue line). While our experiments stop at $x = 0.5$ molar fraction due to solubility issues,[45] we performed MD simulations at $x = 0.9$ as proof of concepts to show the monotonous trend of self-diffusion coefficients beyond the limit of salt solubility.[33]

For what concerns DOSY-NMR experiments, we also report the spectra recorded for each solution (Figure 3 and Table S6 for further details). By looking at the ^{1}H-NMR spectrum (top panel of Figure 3), an overall shift to lower δ is detected with increasing concentration[47] (as highlighted in the inset along the spectrum), whereas in the ^{19}F-NMR spectrum (bottom panel of Figure 3) we first observe a shift from 52.55 ppm in the pure ionic liquid (black line) up to 52.70 ppm for $x = 0.3$ (green line), but then it goes down to 52.65 ppm when going to the $x = 0.5$ composition (blue line). A possible interpretation of the observed variations in chemical shifts with increasing salt concentration can be provided by looking at the shielding factor, which is a measure of the electron density around the nuclei and thus directly affects the chemical shift. There are several terms that contribute to the shielding factor, such as the induced diamagnetic and paramagnetic electronic movement, anisotropy and electric field, which accounts for the electronic circulation in the entire molecule.[48] We can say that the larger transfer of electron density from anions to cations occurring at higher Na salt concentrations can account for the overall decrease of ^{1}H δ values and increase of ^{19}F ones till the $x = 0.3$ composition. However, in the most concentrated system the solvation structure among anions is even tighter, which enhances the surrounding electron density and thus leads to the decreased ^{19}F δ value. We are going to further discuss the solvation structure of the salt-ionic liquid system in the next section of the manuscript.
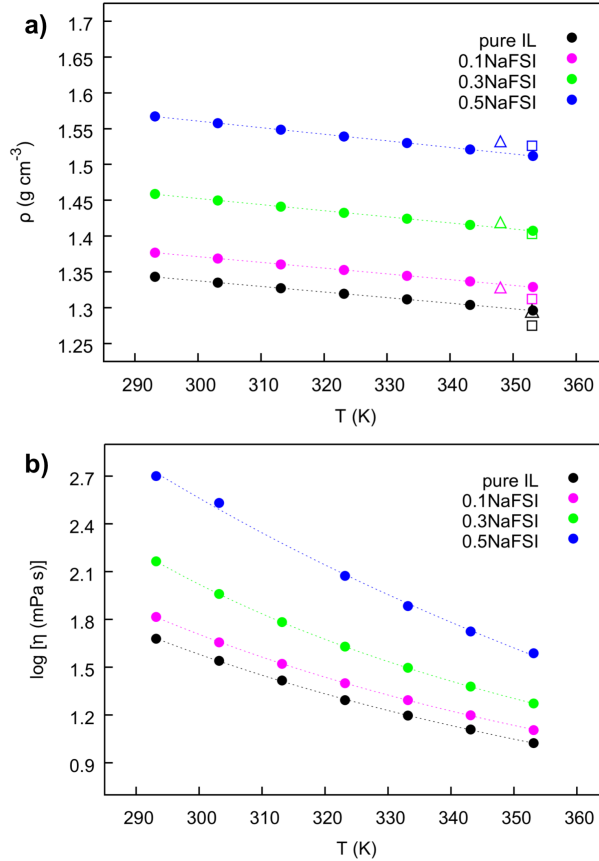
11

Figure 2. Plots of experimental (a) density, ρ, and (b) viscosity, η, of Na[FSI]+[C$_3$C$_1$pyr][FSI] solutions as function of temperature, T, measured for each composition. Dashed lines show the linear and VFTH fits to density and viscosity, respectively. In panel (a) experimental densities from literature[43,44] (triangles) and theoretical densities obtained in this work from polarizable MD models (squares) are also reported for comparison.

The DOSY-NMR experiments allowed us to determine the self-diffusion coefficients of both cation and anion at each concentration and at 298 K. From the data reported in Table II, we observe a slight decrease until $x = 0.3$ and a more important lowering by an order of magnitude at $x = 0.5$, which correlates well with the large increment in viscosity (Figure 2).

The so-obtained self-diffusion coefficients at 298 K together with the viscosities measured at several temperatures served us to compare directly simulation-derived values to experimental ones. This can be easily done by extrapolating the experimental self-diffusion coefficients at 353 K through viscosity taken at 298 K and 353 K, according to the follow-
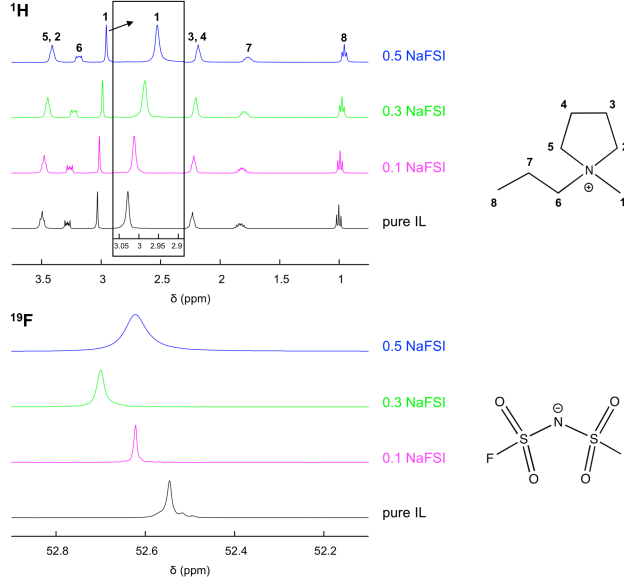
Figure 3. ^{1}H (top) and ^{19}F (bottom) NMR spectra of the sample solutions recorded at 298 K. Inset: zoomed-up region from ^{1}H spectrum.

Table II. Diffusion coefficients, $D_{\mathrm{C_3C_1pyr^+}}$ and $D_{\mathrm{FSI^-}}$, determined from DOSY-NMR experiments at 298 K.

Sample	$D_{\mathrm{C_3C_1pyr^+}}/(\mathrm{m^2\,s^{-1}})$	$D_{\mathrm{FSI^-}}/(\mathrm{m^2\,s^{-1}})$
pure IL	3.27×10^{-11}	3.44×10^{-11}
0.1 Na[FSI]	2.35×10^{-11}	2.57×10^{-11}
0.3 Na[FSI]	1.07×10^{-11}	1.10×10^{-11}
0.5 Na[FSI]	4.06×10^{-12}	2.69×10^{-12}

ing relationship that can be derived from the well-known Stokes-Einstein equation, *i.e.* $D = k_B T/(6\pi\eta r)$.

$$\frac{D(T_1)\eta(T_1)}{T_1} = \frac{D(T_2)\eta(T_2)}{T_2} \tag{3}$$

In this way, we can plot the extrapolated self-diffusion coefficients, $D(353\,\mathrm{K})$, together with the theoretical ones obtained from both polarizable and non-polarizable models as function of Na salt content, as shown in Figure 4 (see Table S1 and S7 for additional details).

From Figure 4, it can be seen that not only self-diffusion coefficients obtained from the
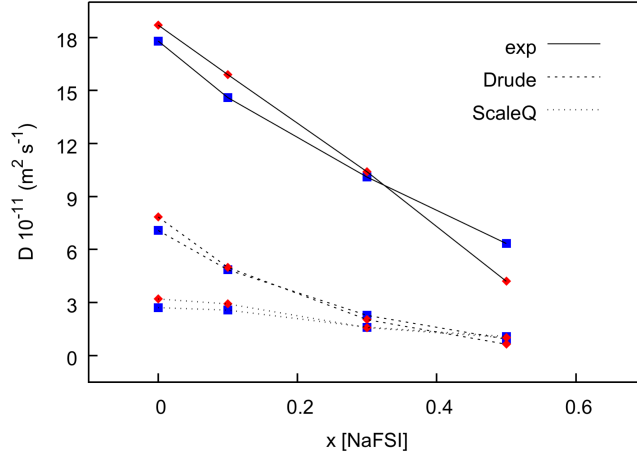
13

Figure 4. Plot of self-diffusion coefficients, D, for cation (blue squares) and anion (red diamonds), as obtained from DOSY-NMR experiments via extrapolation at $353\,\mathrm{K}$ (solid line) and MD simulations with polarizable Drude model (dashed line) and non-polarizable ScaleQ model (dotted line) as function of composition, x [NaFSI]

.

polarizable model are closer to the experimental values, but also that the steep decreasing trend with Na salt content is better reproduced when polarization is taken into account. In conclusion, we can assess the significant beneficial effect of including explicit polarization in the description of the transport properties of sodium and its fundamental role in reconciling the increase in viscosity with the decrease of diffusion of all the ions while the salt content is augmented in the IL-based solution.

B.   Structural analysis

In order to extract structural information that can be useful to examine the coordination shells of sodium, we computed the radial distribution functions (RDF) of oxygen atoms from FSI^- around Na^+ and the corresponding coordination numbers (CN) for each explored composition, with both the fixed-charges and polarizable model (Figure 5). The RDF from the Drude model (Figure 5(b)) shows the first peak at $2.35\,\text{Å}$, representing either monodentate and bidentate geometries (Figure 6). Integration of the RDF to the first valley, *i.e.* to $3.25\,\text{Å}$, leads to CN values increasing from 4.9 to 5.5 when mole fraction of Na salt varies from 0.1 to 0.9. By comparing Figure 5(a) and Figure 5(b), we can clearly say that the narrower

and left-shifted peaks and the CN increase upon concentration detected by the polarizable model suggest that a more refined description of the structure is achieved if polarization is included.
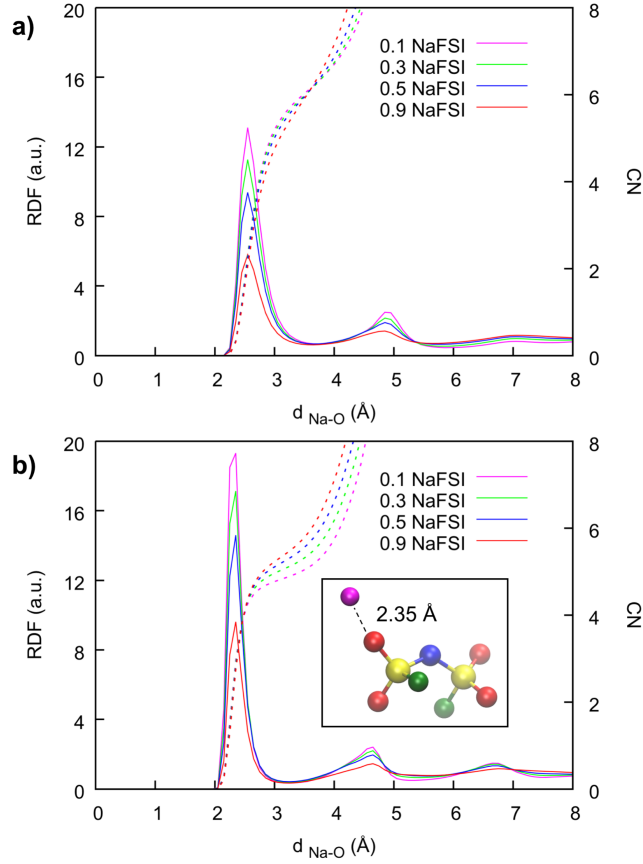

Figure 5. Radial distribution function of Na−O$_{FSI}$ (solid lines) and corresponding coordination number (dashed lines) obtained with the ScaleQ (a) and Drude (b) models. Inset: structural detail of Na−O coordination at 2.35 Å, *i.e.* the first peak of the RDF.

We also explored other possible sodium-anion interactions by looking at RDFs with different coordinating atoms from FSI⁻, *i.e.* nitrogen and fluorine. The RDF of Na−N pairs, Figure 7(a), shows the first peak at 2.45 Å corresponding to a N-monodentate coordination that is stabilized by the neighbour oxygen with a very low CN (∼0.3). On the other hand, the peak at 4.65 Å gives a CN (obtained by integrating up to 5.55 Å) increasing from 4.5 to 5.4 when the salt concentration goes from 0.1 to 0.9. In the RDF of Na−F pairs (Figure 7(b)), the peak at 4.40 Å gives CN from 5.6 to 8.1 (integration up to 5.25 Å). We can conclude that the first solvation shell of sodium is always dominated by oxygen, while nitrogen and fluorine are displaced further out. The coordination number always increases
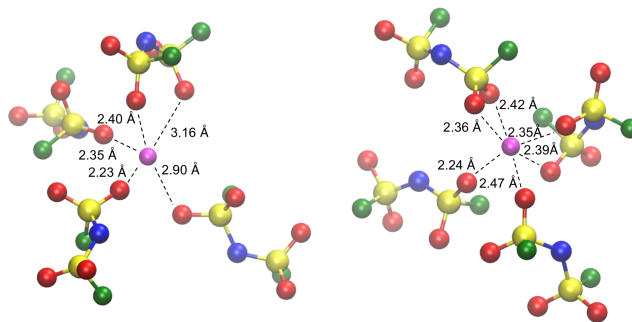
15

Figure 6. (Left) Penta-coordinated geometry around Na with one bidentate FSI$^-$ anion; (Right) hexa-coordinated geometry with two bidentate anions. Na is depicted in purple, O in red, S in yellow,N in blue and F in green.

with Na content, as a result of the larger number of Na$^+$-FSI$^-$ ion pairs.

In order to have a 3D-view of the solvation shells and to see to what extent they change with increasing salt content, we computed spatial distribution functions (SDF) (Figure 8), which are isodensity maps of selected atoms around a central molecule or ion, averaged over an MD trajectory. We chose FSI$^-$ as the central ion and calculated the SDF of three target atom types, namely Na, N(C$_3$C$_1$pyr) and N(FSI). In Figure 8 we see that FSI$^-$ is always surrounded by Na$^+$ at close distances, even at low Na-salt concentration, while C$_3$C$_1$pyr$^+$ is found at slightly longer distances, which is due to the larger size of the pyrrolidinium cation. As a result of cation-separated solvation, FSI$^-$ anions stay closer to the central anion when the smaller Na$^+$ becomes the most abundant cation in the mixture, meaning that FSI−FSI correlations become stronger and anion ordering is more marked at higher salt concentrations. This can also be seen in the RDF of N$_{FSI}$−N$_{FSI}$ reported in Figure S2 and it is in agreement with the analysis of the ^{1}H and ^{19}F NMR spectra based on the electron density around the ions. Looking at the Na−FSI SDF (purple surfaces), a less spread-out distribution is detected at $x = 0.9$ (on the very right side of Figure 8) when compared to less concentrated systems, suggesting a stronger interaction between Na$^+$ and the anions, which most likely accounts for lower sodium mobility.
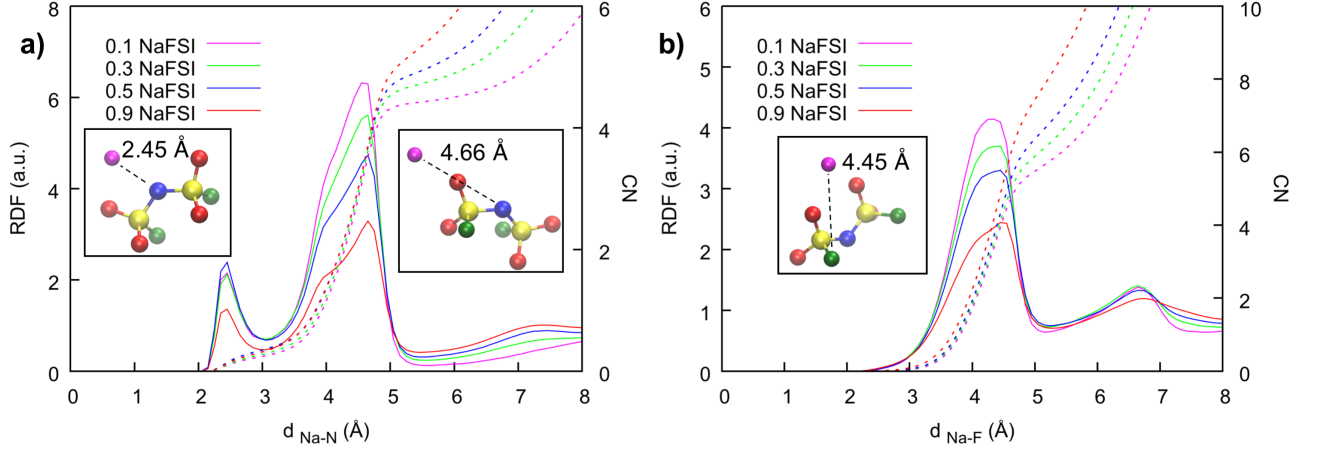
Figure 7. Radial distribution function (solid lines) and corresponding coordination number (dashed lines) of (a) $Na-N_{FSI}$ and (b) $Na-F_{FSI}$ distances.
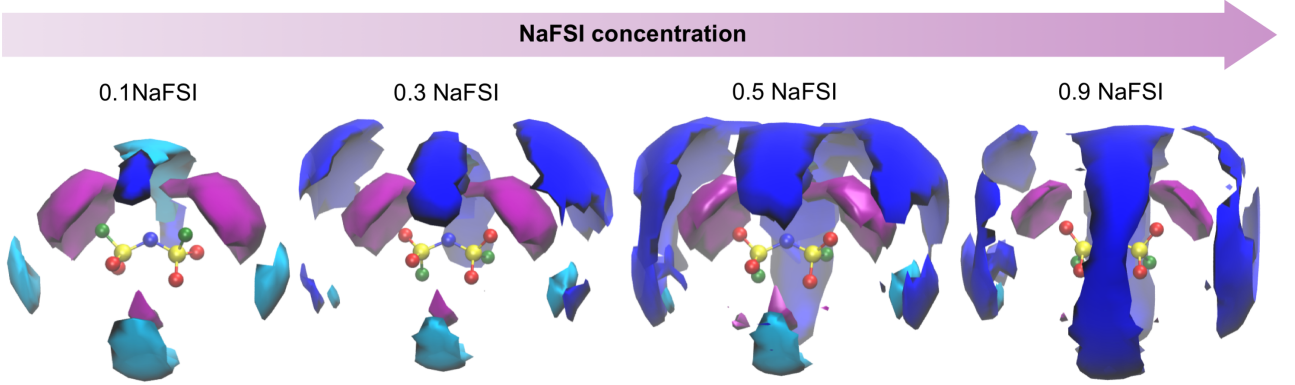

Figure 8. Spatial distribution functions of FSI^- (blue), $C_3C_1pyr^+$ (cyan) and Na^+ (purple) around central FSI^- at different compositions. We consider N as the atom whose density is computed in both cation and anion. The isosurface is plotted at 1.7, 4.5 and 7.3 times the average density of FSI^-, $C_3C_1pyr^+$ and Na^+, respectively.

IV.   CONCLUSIONS

In this work we report a joint theoretical and experimental study of sodium transport properties at different concentrations in the $[C_3C_1pyr][FSI]$ ionic liquid. Understanding ion transport is essential to boost the deployment of ionic liquids as electrolytes for sustainable and high-performance energy-storage devices, such as Na-ion batteries. Our study aims to give further insights in this field that can be sum up as follows:

- explicit polarization does affect the reliability of the theoretical model, especially when it concerns large molecular ions interacting via non-covalent forces. We compare our polarizable model for the $Na[FSI]+[C_3C_1pyr][FSI]$ system as obtained from the existent atomistic force field for ILs with a commonly adopted non-polarizable model and show that more accurate predictions of dynamic properties and structural quantities are provided if polarization is taken into account;

- direct comparison of theoretical predictions with experimental results represents an unambiguous way to outline the relevance of polarization in MD simulations. We provide both physico-chemical characterization of our solutions (in terms of density and viscosity) and diffusion coefficients determined from pulse field gradient NMR experiments;

- structural analysis of solvation layers provides insights into sodium mobility that seems to be inhibited at higher concentration due to formation of Na^+-FSI^- ion pairs.

Our study may contribute to future works aiming to investigate similar IL-based electrolytes for important applications in novel energy-storage and sensor technologies. The use of polarizable force fields can be extended to even more complex materials where the atomistic description is key to unveil the mechanism of sodium transport.

ACKNOWLEDGMENTS

REFERENCES

[1] D. Larcher and J.-M. Tarascon, "Towards greener and more sustainable batteries for electrical energy storage," Nature Chemistry **7**, 19 (2014).

[2]J. B. Goodenough and K.-S. Park, "The li-ion rechargeable battery: A perspective," Journal of the American Chemical Society **135**, 1167–1176 (2013).

[3]J. B. Goodenough and Y. Kim, "Challenges for rechargeable li batteries," Chemistry of Materials **22**, 587–603 (2010).

[4]B. Scrosati and J. Garche, "Lithium batteries: Status, prospects and future," Journal of Power Sources **195**, 2419 – 2430 (2010).

[5]J.-Y. Hwang, S.-T. Myung, and Y.-K. Sun, "Sodium-ion batteries: present and future," Chemical Society Reviews **46**, 3529–3614 (2017).

[6]L. P. Wang, L. Yu, X. Wang, M. Srinivasan, and Z. J. Xu, "Recent developments in electrode materials for sodium-ion batteries," Journal of Material Chemistry A **3**, 9353–9378 (2015).

[7]Z. Dai, U. Mani, H. T. Tan, and Q. Yan, "Advanced cathode materials for sodium-ion batteries: What determines our choices?" Small Methods **1**, 1700098 (2017).

[8]E. Quartarone and P. Mustarelli, "Electrolytes for solid-state lithium rechargeable batteries: recent advances and perspectives," Chemical Society Reviews **40**, 2525–2540 (2011).

[9]A. Lewandowski and A. Świderska-Mocek, "Ionic liquids as electrolytes for li-ion batteries—an overview of electrochemical studies," Journal of Power Sources **194**, 601 – 609 (2009).

[10]J. R. Nair, F. Colò, A. Kazzazi, M. Moreno, D. Bresser, R. Lin, F. Bella, G. Meligrana, S. Fantini, E. Simonetti, G. B. Appetecchi, S. Passerini, and C. Gerbaldi, "Room temperature ionic liquid (rtil)-based electrolyte cocktails for safe, high working potential li-based polymer batteries," Journal of Power Sources **412**, 398 – 407 (2019).

[11]L. Porcarelli, P. S. Vlasov, D. O. Ponkratov, E. I. Lozinskaya, D. Y. Antonov, J. R. Nair, C. Gerbaldi, D. Mecerreyes, and A. S. Shaplov, "Design of ionic liquid like monomers towards easy-accessible single-ion conducting polymer electrolytes," European Polymer Journal **107**, 218 – 228 (2018).

[12]P. Walden, "Molecular weights and electrical conductivity of several fused salts," Bulletin of the Imperial Academy of Sciences (Saint Petersburg) **1800**, 405–422 (1914).

[13]N. V. Plechkova and K. R. Seddon, "Applications of ionic liquids in the chemical industry," Chemical Society Reviews **37**, 123–150 (2008).

[14]P. Wasserscheid and T. Welton, "Ionic liquids in synthesis," Wiley , 380 (2003).

[15]L. F. Lepre, D. Andre, S. Denis-Quanquin, A. Gautier, A. A. H. Pádua, and

M. Costa Gomes, "Ionic liquids can enable the recycling of fluorinated greenhouse gases," ACS Sustainable Chemistry & Engineering **7**, 16900–16906 (2019).

[16]M. Armand, F. Endres, D. R. MacFarlane, H. Ohno, and B. Scrosati, "Ionic-liquid materials for the electrochemical challenges of the future," Nature Materials **8**, 621–629 (2009).

[17]A. Somers, P. Howlett, D. MacFarlane, and M. Forsyth, "A review of ionic liquid lubricants," Lubricants **1**, 3–21 (2013).

[18]M. P. Scott, C. S. Brazel, M. G. Benton, J. W. Mays, J. D. Holbrey, and R. D. Rogers, "Application of ionic liquids as plasticizers for poly(methyl methacrylate)," Chemical Communications , 1370–1371 (2002).

[19]T. F. Miller, Z.-G. Wang, G. W. Coates, and N. P. Balsara, "Designing polymer electrolytes for safe and high capacity rechargeable lithium batteries," Accounts of Chemical Research **50**, 590–593 (2017).

[20]F. Chen and M. Forsyth, "Elucidation of transport mechanism and enhanced alkali ion transference numbers in mixed alkali metal–organic ionic molten salts," Physical Chemistry Chemical Physics **18**, 19336–19344 (2016).

[21]W. L. Jorgensen, D. S. Maxwell, and J. Tirado-Rives, "Development and testing of the opls all-atom force field on conformational energetics and properties of organic liquids," Journal of the American Chemical Society **118**, 11225–11236 (1996).

[22]J. N. Canongia Lopes, J. Deschamps, and A. A. H. Pádua, "Modeling ionic liquids using a systematic all-atom force field," The Journal of Physical Chemistry B **108**, 2038–2047 (2004).

[23]J. N. Canongia Lopes and A. A. H. Pádua, "Cl&p: A generic and systematic force field for ionic liquids modeling," Theoretical Chemistry Accounts **131** (2012).

[24]A. A. H. Pádua, "Resolving dispersion and induction components for polarisable molecular simulations of ionic liquids," The Journal of Chemical Physics **146**, 204501 (2017).

[25]B. L. Bhargava and S. Balasubramanian, "Refined potential model for atomistic simulations of ionic liquid [bmim][pf6]," The Journal of Chemical Physics **127**, 114510 (2007).

[26]V. Chaban, "Polarizability versus mobility: atomistic force field for ionic liquids," Physical Chemistry Chemical Physics **13**, 16055–16062 (2011).

[27]Y. Zhang and E. J. Maginn, "A simple aimd approach to derive atomic charges for condensed phase simulation of ionic liquids," The Journal of Physical Chemistry B **116**, 10036–10048 (2012).

[28]D. Bedrov, J.-P. Piquemal, O. Borodin, A. D. MacKerell, B. Roux, and C. Schröder, "Molecular dynamics simulations of ionic liquids and electrolytes using polarizable force fields," Chemical Reviews **119**, 7940–7995 (2019).

[29]K. Goloviznina, J. N. Canongia Lopes, M. Costa Gomes, and A. A. H. Pádua, "Transferable, polarizable force field for ionic liquids," Journal of Chemical Theory and Computation **15**, 5858–5871 (2019).

[30]C. Ding, T. Nohira, K. Kuroda, R. Hagiwara, A. Fukunaga, S. Sakai, K. Nitta, and S. Inazawa, "Nafsa–c1c3pyrfsa ionic liquids for sodium secondary battery operating over a wide temperature range," Journal of Power Sources **238**, 296 – 300 (2013).

[31]Z. Hu, J. Vatamanu, O. Borodin, and D. Bedrov, "A comparative study of alkylimidazolium room temperature ionic liquids with fsi and tfsi anions near charged electrodes," Electrochimica Acta **145**, 40 – 52 (2014).

[32]A. Basile, M. Hilder, F. Makhlooghiazad, C. Pozo-Gonzalo, D. R. MacFarlane, P. C. Howlett, and M. Forsyth, "Ionic liquids and organic ionic plastic crystals: Advanced electrolytes for safer high performance sodium energy storage technologies," Advanced Energy Materials **8**, 1703491 (2018).

[33]F. Chen, P. Howlett, and M. Forsyth, "Na-ion solvation and high transference number in superconcentrated ionic liquid electrolytes: A theoretical approach," The Journal of Physical Chemistry C **122**, 105–114 (2018).

[34]C. Schröder and O. Steinhauser, "Simulating polarizable molecular ionic liquids with drude oscillators," The Journal of Chemical Physics **133**, 154511 (2010).

[35]G. Lamoureux and B. Roux, "Modeling induced polarization with classical drude oscillators: Theory and molecular dynamics simulation algorithm," The Journal of Chemical Physics **119**, 3025–3039 (2003).

[36]J. A. Lemkul, J. Huang, B. Roux, and A. D. MacKerell, "An Empirical Polarizable Force Field Based on the Classical Drude Oscillator Model: Development History and Recent Applications," Chem. Rev. **116**, 4983–5013 (2016).

[37]E. Heid, A. Szabadi, and C. Schröder, "Quantum mechanical determination of atomic polarizabilities of ionic liquids," Physical Chemistry Chemical Physics **20**, 10992–10996 (2018).

[38]S. J. Plimpton, "Fast Parallel Algorithms for Short-Range Molecular Dynamics," J. Comput. Phys. **117**, 1–19 (1995).

[39] A. Dequidt, J. Devémy, and A. A. H. Pádua, "Thermalized drude oscillators with the lammps molecular dynamics simulator," Journal of Chemical Information and Modeling **56**, 260–268 (2015).

[40] A. A. H. Pádua, fftool , github.com/agiliopadua/fftool (2013).

[41] L. Martínez, R. Andrade, E. G. Birgin, and J. M. Martínez, "Packmol: A package for building initial configurations for molecular dynamics simulations," J. Comput. Chem. **30**, 2157–2164 (2009).

[42] C. Cadena, Q. Zhao, Q. R. Snurr, and J. E. Maginn, "Molecular modeling and experimental studies of thermodynamic and transport properties of pyridiunium-based ionic liquids," Journal of Physical Chemistry B **110**, 2821 – 2832 (2006).

[43] K. Hayamizu, S. Tsuzuki, S. Seki, K. Fujii, M. Suenaga, and Y. Umebayashi, "Studies on the translational and rotational motions of ionic liquids composed of n-methyl-n-propyl-pyrrolidinium (p13) cation and bis(trifluoromethanesulfonyl)amide and bis(fluorosulfonyl)amide anions and their binary systems including lithium salts," The Journal of Chemical Physics **133**, 194505 (2010).

[44] K. Matsumoto, Y. Okamoto, T. Nohira, and R. Hagiwara, "Thermal and transport properties of na[n(so2f)2]–[n-methyl-n-propylpyrrolidinium][n(so2f)2] ionic liquids for na secondary batteries," The Journal of Physical Chemistry C **119**, 7648–7655 (2015).

[45] M. Forsyth, H. Yoon, F. Chen, H. Zhu, D. R. MacFarlane, M. Armand, and P. C. Howlett, "Novel na+ ion diffusion mechanism in mixed organic–inorganic ionic liquid electrolyte leading to high na+ transference number and stable, high rate electrochemical cycling of sodium cells." The Journal of Physical Chemistry C **120**, 4276–4286 (2016).

[46] M. L. F. Nascimento and C. Aparicio, "Data classification with the vogel–fulcher–tammann–hesse viscosity equation using correspondence analysis," Physica B: Condensed Matter **398**, 71 – 77 (2007).

[47] T. Yim, C. Y. Choi, J. Mun, S. M. Oh, and Y. G. Kim, "Synthesis and properties of acyclic ammonium-based ionic liquids with allyl substituents as electrolytes," Molecules **14**, 1840–1851 (2009).

[48] J. Keeler, "Understanding nmr spectroscopy," Wiley **2nd Edition** (2010).